

pubs.acs.org/journal/apchd5 Letter

# Molybdenum Silicide Superconducting Nanowire Single-Photon Detectors on Lithium Niobate Waveguides

Marco Colangelo,\* Di Zhu, Linbo Shao, Jeffrey Holzgrafe, Emma K. Batson, Boris Desiatov, Owen Medeiros, Matthew Yeung, Marko Loncar,\* and Karl K. Berggren\*



Cite This: ACS Photonics 2024, 11, 356-361



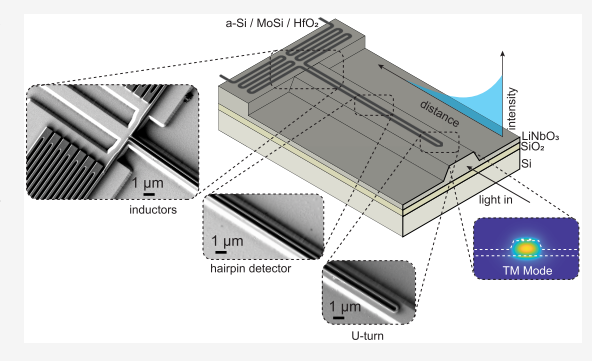
**ACCESS** I

III Metrics & More

Article Recommendations

s Supporting Information

ABSTRACT: We demonstrate a molybdenum silicide superconducting nanowire single-photon detector heterogeneously integrated onto a thin-film lithium niobate waveguide. The detector achieves approximately 50% on-chip detection efficiency at 1550 nm with a jitter of 82 ps when measured at 0.78 K. This demonstration showcases the integration of an amorphous superconductor utilizing conventional fabrication processes without strict cooling and substrate requirements. This paves the way for the integration of additional superconducting electronic components, potentially realizing the full promise of integrated quantum photonic circuits.



KEYWORDS: SNSPD, thin-film lithium niobate (TFLN), heterogeneous integration, quantum photonics, applied superconductivity

## **■ INTRODUCTION**

Efficient detection of extremely faint light signals remains one of the critical challenges in the development of integrated quantum photonic circuits. Superconducting nanowire single-photon detectors (SNSPDs) are the leading photon-counting technology, offering high system detection efficiency, low dark counts, and unrivaled timing resolution at infrared wavelengths. The heterogeneous integration of these devices is crucial to fully exploit the high throughput and low loss offered by integrated photonics.

Waveguide-integrated superconducting nanowire single-photon detectors (WGSNSPDs) rely on the efficient coupling between the evanescent field of the guided optical mode and the superconducting nanowire, which is placed directly atop optical waveguides. Owing to their reduced footprint, these architectures offer several advantages, including improved timing resolution, reduced reset time, and higher count rates. WGSNSPDs have been successfully implemented on various photonic platforms, such as silicon-on-insulator, 7,8 silicon nitride, 9,10 aluminum nitride, 11 diamond, 2 gallium arsenide, and tantalum oxide. 14

Thin-film lithium niobate (TFLN) is a promising platform for quantum photonics due to its low optical loss <sup>15</sup> and large all-optical and electro-optic nonlinearities. <sup>16–19</sup> Integrating SNSPDs into this platform could significantly advance the development of fully integrated photonic circuits. However, notable challenges exist. <sup>19</sup> First, the deposition process of high-quality superconducting films must be tailored to avoid excessive substrate heating to be compatible with lithium niobate. To address this challenge, recent studies have

introduced low-temperature superconducting thin-film deposition methods that are suitable for integration purposes.<sup>20-22</sup> Second, aggressive dry etching and wet cleaning, essential for optimal waveguide patterning, might compromise the nanowire fabrication yield and overall detector performance. Depending on the chosen process flow, several mitigation strategies can be implemented. In detector-first methodologies (where nanowires are fabricated before waveguide etching), encapsulation layers can be applied to reduce nanowire degradation.<sup>22</sup> In contrast, waveguide-first methods (where nanowires are produced after waveguide etching) naturally circumvent exposure to aggressive chemicals. However, this method might lead to waveguide quality degradation from the nanowire fabrication process, increasing the optical losses. Additionally, the waveguide's surface roughness can influence the detector yield.<sup>21</sup> In such cases, buffer layers<sup>20</sup> offer protection to the waveguides during subsequent processing while also potentially reducing surface roughness. The nanowire yield can also be improved by employing amorphous superconductors as they have less stringent substrate requirements.<sup>22</sup>

Received: November 9, 2023 Revised: January 9, 2024 Accepted: January 10, 2024 Published: January 16, 2024





Using a waveguide-first approach, hafnium oxide buffer layer, and atomic-layer deposited niobium nitride, Sayem et al. demonstrated an integrated SNSPD on lithium niobate with a 46% on-chip detection efficiency and 32 ps jitter. Using a detector-first approach with a silicon oxide protection layer and niobium—titanium-nitride, Lomonte et al. demonstrated a 27% on-chip detection efficiency and 17.1 ps jitter.

In this paper, we demonstrate the heterogeneous integration of a superconducting nanowire single photon detector on a thin-film lithium niobate waveguide. We employ a waveguidefirst approach with a conformal hafnium oxide buffer layer to mitigate fabrication-induced waveguide loss. We integrated a room-temperature-sputtered amorphous molybdenum silicide (MoSi) superconducting film to improve nanowire yield. This amorphous superconducting material has a relatively high critical temperature and kinetic inductance and is well suited for integrating other superconducting devices with no strict requirements on cooling, operation temperatures, and substrate. Our integrated SNSPD achieved an OCDE of 50.2% and a system jitter of 82 ps. In the following, we discuss the design and fabrication of our integrated devices. We show the results for the on-chip detection efficiency and timing resolution. We conclude with a brief discussion and outlook.

## DESIGN AND FABRICATION

Figure 1a shows a sketch of our photonic integrated circuit (PIC) with an integrated detector. The photonic structure consists of an input grating coupler interfaced to a 3 dB Y-splitter, shown in subfigure (i). One output of the Y-splitter is connected to another nominally identical grating coupler, completing a loop-back monitoring structure. The other output is a 400  $\mu \rm m$  long waveguide. The superconducting detector is a nanowire hairpin fabricated on top of the waveguide, shown in (ii) connected on each side to a meandering nanowire inductor terminated to contact pads.

The PIC was fabricated on a commercial X-cut lithiumniobate-on-insulator wafer (NanoLN). The TFLN device layer was 600 nm thick on top of a 2  $\mu$ m thick buried thermal oxide on a silicon handle wafer. The photonic circuit was patterned in hydrogen silsesquioxane (HSQ) with electron beam lithography (EBL) and transferred to the TFLN layer using Ar+-based reactive ion etching (RIE). The etching depth was 350 nm. A 10 nm thick hafnium dioxide layer was deposited by atomic layer deposition, at 90 °C. This buffer layer protects the TFLN devices from further processing.<sup>20</sup> Moreover, we also hypothesize a smoothing of the residual roughness based on studies with other ALD-deposited thin films, e.g., Al<sub>2</sub>O<sub>3</sub><sup>23</sup> and TiO<sub>2</sub>. <sup>24,25</sup> A 6.3 nm thick MoSi film was cosputtered on the substrate at room temperature, protected by a 2 nm thick sputtered amorphous silicon capping layer. The Mo/Si sputtering conditions were tuned toward a higher silicon content (50 W DC/120 W RF) to reduce the crystalline fraction, as demonstrated in our previous investigations. 26,2 The sheet resistance was  $R_s = 475 \ \Omega$  per square and the critical temperature  $T_c = 3.4$  K, both measured on a monitor chip. Electrical contacts were fabricated with aligned direct writing photolithography, followed by two angled evaporation of a 10 nm-thick titanium adhesion layer and a 100 nm-thick gold electrical layer, followed by liftoff. The nanowire detector was patterned in HSQ with aligned EBL and transferred into the MoSi with RIE in CF<sub>4</sub> chemistry.

Our detector was designed as a U-shaped hairpin with a width of 100 nm and a spacing of 200 nm. These dimensions

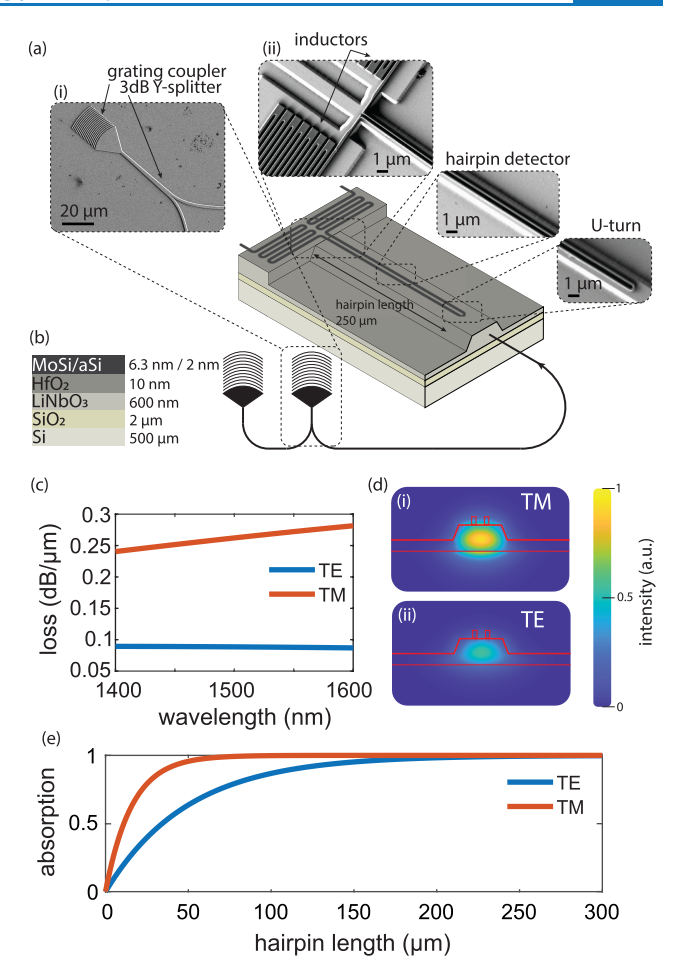


**Figure 1.** Device architecture, design, and simulation. (a) Scanning electron micrographs of the devices (hairpin and PIC), accompanied by an artist's sketch. (b) Materials stack. (c) Simulated optical loss for TE and TM modes as a function of the wavelength. (d) Simulated TE and TM modes at 1550 nm. (e) Simulated total absorption in the waveguide as a function of the hairpin length for TE and TM modes at 1550 nm.

were chosen to reduce the challenges in aligning the hairpin to the 1  $\mu$ m wide waveguide during electron-beam lithography.

We simulated the waveguide fundamental modes and their optical losses in the presence of the hairpin. We included all of the layers in the stack (Figure 1b), using the measured index of refraction for the superconducting film (see Supporting Information) and nominal values for the other materials. Figure 1c shows the optical absorption as a function of the wavelength for the TM (i) and TE (ii) modes. Here we assume absorption only in the superconducting layer. The modes at 1550 nm are shown in Figure 1(d)-(i) and (d)-(ii). At this wavelength, the absorptions for TE and TM modes are 0.089 and 0.272 dB  $\mu$ m<sup>-1</sup>, respectively. To ensure near-unity absorption for both modes (Figure 1e), we designed the length of our hairpin to be 250  $\mu$ m.

## ■ RESULTS AND DISCUSSION

We measured our device in a closed-loop cryostat with a base temperature of  $T=0.78~\rm K$ . A sketch of the setup and detailed specifications of the instruments are available in the Supporting Information. Our measurement setup included an off-chip cryogenic inductive shunt to extend the biasing margin and saturation plateau. The inductive shunt provided a low

resistivity path for low-frequency components of the detection pulse and prevented the detector from latching prematurely. With this device, we improved the detector bias margin by about 15%, increasing from a switching current of 9  $\mu$ A without the shunt to 10.5  $\mu$ A in the presence of the shunt. See Supporting Information for a comparison.

Figure 2a shows a characteristic output pulse (the plot shows the average over ten pulses) for the 250  $\mu$ m long hairpin. The

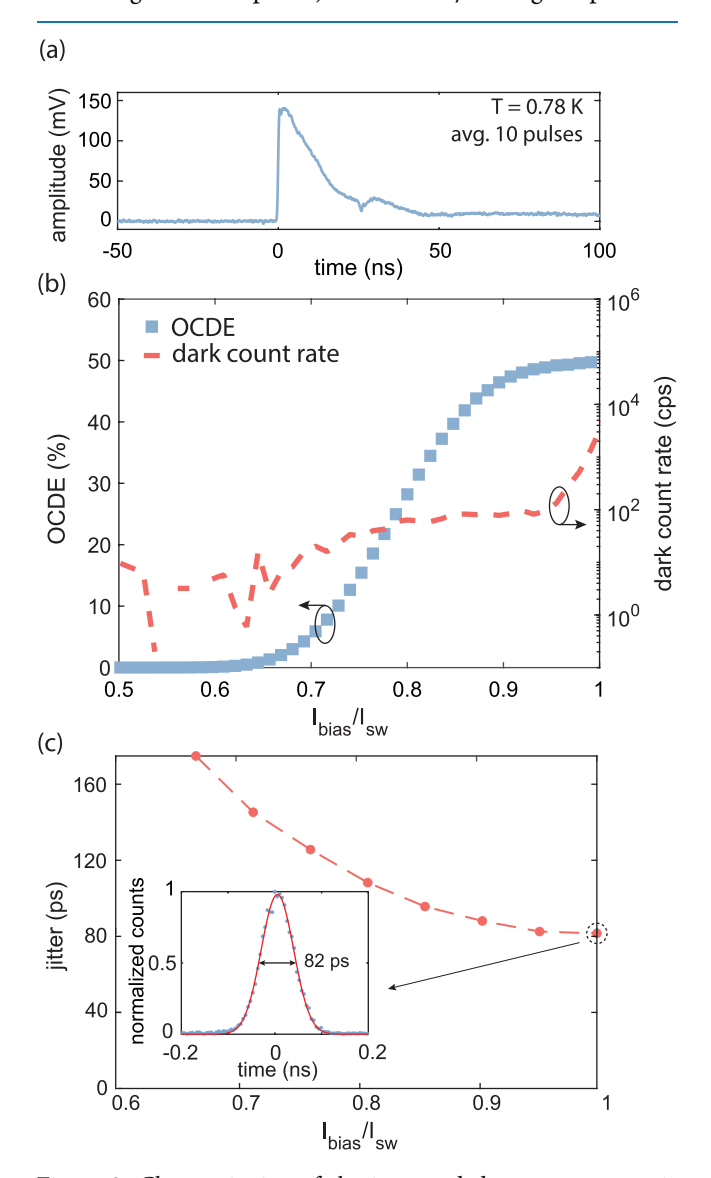


**Figure 2.** Characterization of the integrated detector at cryogenic temperature. (a) Detector output pulse at 0.78 K. The waveform is an average of 10 pulses. (b) On-chip detection efficiency curve for our 250  $\mu$ m long hairpin detector tested at 0.78 K with 1550 nm photons. (c) System jitter as a function of the bias current. The inset shows our lowest measured jitter, 82 ps.

bump at about 30 ns is attributed to reflections from the amplifier. The reset time constant is  $\tau = 14.5$  ns, extracted from fitting the relaxation of the pulse with an exponential function. The inductive shunt accelerates the detector reset dynamics. More details are available in the Supporting Information.

We characterized the on-chip detection efficiency (OCDE) by coupling light into the waveguide through the input grating coupler using a fiber array mounted on a three-axis piezo positioner, thermalized to the coldest stage of the cryostat. The

coupling was performed at room temperature, monitored during cooldown, and optimized at the base temperature using the loop-back structure. More details on the procedure are available in the Supporting Information. The OCDE was estimated with the following relation:

$$OCDE = \frac{PCR - DCR}{\Phi_q}$$
 (1)

where PCR is the count rate of the detector measured with illumination, DCR is the dark count rate, and  $\Phi_q$  is the photon flux in the detector waveguide. The photon flux was estimated with the following relation:

$$\Phi_{q} = \frac{1}{h\nu} \sqrt{\frac{\eta_{\text{attn}}^{2} P_{\text{in}} P_{\text{out}}}{2}}$$
(2)

where  $h\nu$  is the energy associated with a photon of frequency  $\nu$ ,  $\eta_{\rm attn}$  is the attenuation applied with the variable optical attenuator,  $P_{\rm in}$  is the supplied optical power, measured at the input of the cryostat, and  $P_{\rm out}$  is the optical power at the output of the loopback structure, measured at the cryostat level. Both  $P_{\rm in}$  and  $P_{\rm out}$  are measured before applying the optical attenuation,  $\eta_{\rm attn}$ , required for OCDE characterization. These relations assume a perfect 3 dB Y-splitter, identical grating couplers, and negligible waveguide loss. Figure 2b shows the measured OCDE. Our device had a saturated OCDE of about 50.2%, with a 100 s<sup>-1</sup> dark count rate at 95% of the bias range on the plateau. We estimate the uncertainty of the reported OCDE to be  $\pm 7.1\%$ , dominated by the uncertainty of the power meter. See Supporting Information for a discussion on the uncertainty estimation.

For a 250  $\mu$ m long hairpin, we would have expected a unity OCDE. We attribute this discrepancy to a combination of two potential issues. First, the efficiency calculation assumed a perfectly balanced 3 dB Y-splitter, perfect alignment, and identical grating couplers. In reality, alignment, polarization, and fabrication issues are expected to contribute to ≈1 dB variation between grating coupler insertion loss. Moreover, a 5% splitter unbalance could result in an  $\pm 15\%$  relative discrepancy in efficiency. Second, our calculation assumed zero intrinsic waveguide and materials optical loss, except for the superconductor. While the propagation loss in the lithium niobate waveguide is expected to be less than 0.2 dB/cm, 15 additional losses induced by further fabrication or in the buffer layers can degrade the measured efficiency. The reflections at the waveguide transition into the hairpin region do not constitute a significant contribution to the efficiency. See Supporting Information for additional details.

We measured the timing resolution of the integrated detector. Figure 2c shows the system jitter as a function of the bias current. The lowest jitter was 82 ps, obtained at the maximum bias current of the detector before relaxation oscillations. The jitter saturated with the bias current at a relatively large value compared to other results on the same platform. We attributed this effect to two main elements. First, the detector had a total length of about 0.5 mm with a relatively high kinetic inductance (about 200 pH per square) due to the reduced critical temperature of the film. Therefore, we expect the geometric contribution to the timing jitter to be particularly significant in our detector. We estimate a contribution of  $\approx$ 61 ps (see Supporting Information for details). Second, our measurement setup was not optimized for low-jitter measurements as we did not use cryogenic amplifiers.

We estimate the electronic noise contribution to the timing jitter to be  $\approx\!\!25$  ps (see Supporting Information for details). We expect the implementation of a differential readout strategy  $^{28}$  and the inclusion of low-noise cryogenic electronics to improve our jitter metric to below 20 ps, as demonstrated in other works.  $^{22,28}$ 

# SUMMARY AND CONCLUSIONS

In summary, we demonstrated a MoSi hairpin SNSPD integrated on a thin-film lithium niobate waveguide. At T=0.78 K, we obtained a saturated OCDE of 50.2% with an uncertainty of 7.1%. Our efficiency is comparable with other demonstrations using similar fabrication methods and materials. Unfortunately, geometric factors and our measurement setup limited the timing jitter to 82 ps.

Wide-scale adoption of these integrated detectors for quantum applications, however, requires enhanced performance in both OCDE (>90%) and timing jitter (<20 ps). To improve the efficiency metric and address the additional sources of inefficiency in our measurement, it is crucial to decouple the optical absorption of the hairpin from the propagation loss of the HfO2-coated lithium-niobate waveguide and the insertion loss and nonidealities of the photonic components. This differentiation can be achieved by integrating loss calibration devices, such as microring resonators,  $^{15,29}$  on the same chip, as well as by measuring a statistically relevant set of photonic devices to characterize their fabricated behavior and quantify their deviation from the intended design. Monitoring the output power from the SNSPD branch through an additional loop-back could also help characterize the loss. However, this measurement is feasible only at relatively high optical power due to the limited sensitivity of classical detectors.

Ultimately, the current architecture based on the traditional hairpin-waveguide-coupling strategy<sup>30</sup> will lead to a trade-off between the efficiency metric, proportional to the length of the wire (Figure 1e), and the timing metrics (reset dynamics, count rate, and jitter), which are inversely proportional to the length. A strategy to reduce the length of the wire, improve the timing metrics, and simultaneously obtain high efficiency consists of optimizing the waveguide design and nanowire placement to increase the mode leakage and enhance the evanescent coupling.<sup>31</sup> The residual geometric jitter could be canceled with differential readout and the reset time quenched with an external circuit.<sup>32</sup> Another approach involves placing a much shorter nanowire within a high-quality-factor photonic crystal (PhC) cavity, capitalizing on the concept of coherent perfect absorber.<sup>33</sup> This approach was demonstrated with SNSPDs on a silicon-on-insulator platform, using 1D and 2D PhCs. 8,34,35 Given the recent advancement in thin-film lithium niobate photonic device design and fabrication technology, <sup>19</sup> we believe that SNSPDs integration with PhCs on this platform could be a promising solution to enhance efficiency and timing resolution.

Our work demonstrates a viable approach to the heterogeneous integration of single-photon detectors on the lithium niobate platform using conventional materials and fabrication processes. Molybdenum silicide can be deposited at room temperature, has a reasonably high critical temperature (>3 K), and a high London penetration depth leading to a high kinetic inductance (>100 pH per square). These characteristics are well suited for realizing and integrating other superconducting devices with no strict requirements on cooling and

operation temperatures. These include digital, <sup>36–38</sup> and microwave<sup>39</sup> electronic devices. Their monolithic integration with SNSPDs could lead to the realization of comprehensive circuits for on-chip quantum information processing, realizing the full potentials of integrated quantum photonics. <sup>19,40</sup>

#### ASSOCIATED CONTENT

# Supporting Information

The Supporting Information is available free of charge at https://pubs.acs.org/doi/10.1021/acsphotonics.3c01628.

Description of the material parameters, measurement setup, optimization of the optical alignment, estimation of the optical losses, characterization of the DC properties of the device and shunting circuit, and the estimation of uncertainties (PDF)

## AUTHOR INFORMATION

## **Corresponding Authors**

Marco Colangelo — Research Laboratory of Electronics, Massachusetts Institute of Technology, Cambridge, Massachusetts 02139, United States; Present Address: Electrical and Computer Engineering Department, Northeastern University, Boston 02115, U.S.A; ⊙ orcid.org/0000-0001-7611-0351; Email: ma.colangelo@northeastern.edu

Marko Loncar — John A. Paulson School of Engineering and Applied Science, Harvard University, Cambridge, Massachusetts 02138, United States; Email: loncar@seas.harvard.edu

Karl K. Berggren — Research Laboratory of Electronics, Massachusetts Institute of Technology, Cambridge, Massachusetts 02139, United States; ⊚ orcid.org/0000-0001-7453-9031; Email: berggren@mit.edu

# **Authors**

Di Zhu — Research Laboratory of Electronics, Massachusetts Institute of Technology, Cambridge, Massachusetts 02139, United States; John A. Paulson School of Engineering and Applied Science, Harvard University, Cambridge, Massachusetts 02138, United States; Present Address: Department of Materials Science and Engineering, National University of Singapore, Singapore 117575, Singapore.

Linbo Shao — John A. Paulson School of Engineering and Applied Science, Harvard University, Cambridge, Massachusetts 02138, United States; Present Address: Bradley Department of Electrical and Computer Engineering, Virginia Tech, Blacksburg, VA, U.S.A.

Jeffrey Holzgrafe — John A. Paulson School of Engineering and Applied Science, Harvard University, Cambridge, Massachusetts 02138, United States; Present Address: HyperLight Corporation, Cambridge, Massachusetts 02138, U.S.A.

Emma K. Batson — Research Laboratory of Electronics, Massachusetts Institute of Technology, Cambridge, Massachusetts 02139, United States; orcid.org/0000-0002-7871-5984

Boris Desiatov — John A. Paulson School of Engineering and Applied Science, Harvard University, Cambridge, Massachusetts 02138, United States; Present Address: Faculty of Engineering, Bar-Ilan University,

Ramat-Gan, 52900 Israel.; o orcid.org/0000-0001-7916-8727

Owen Medeiros — Research Laboratory of Electronics, Massachusetts Institute of Technology, Cambridge, Massachusetts 02139, United States

Matthew Yeung — Research Laboratory of Electronics, Massachusetts Institute of Technology, Cambridge, Massachusetts 02139, United States

Complete contact information is available at: https://pubs.acs.org/10.1021/acsphotonics.3c01628

#### **Author Contributions**

M.C. and D.Z. conceived and designed the device. M.C. performed the experiments. M.C., D.Z., J.H., L.S., O.M., B.D., E.B., and M.Y. fabricated the devices. M.C., D.Z., and J.H. performed the simulations. K.K.B. and M.L. supervised the project. M.C. wrote the paper with input from all authors.

#### **Funding**

This research was sponsored by the National Science Foundation Grant ECCS102137723. M.C. was supported by the MIT Claude E. Shannon Award. D.Z. was supported by Harvard Quantum Initiative Postdoctoral Fellowship. M.Y. acknowledges support from the National Science Foundation Graduate Research Fellowship Program, Grant No. 1745302, and the MathWorks Fellowship. The opinions and views expressed in this publication are from the authors and not necessarily from the National Science Foundation or Math-Works.

#### Notes

The authors declare the following competing financial interest(s): J.H. is currently involved in the development of lithium niobate technology at HyperLight Corporation.

## ACKNOWLEDGMENTS

The authors acknowledge P. D. Keathley, A. Simon, and R. Foster for reviewing the manuscript. The authors thank Dr. Bartholomeus Machielse for the atomic layer deposition of the buffer layer.

# REFERENCES

- (1) Moody, G.; Sorger, V. J; Blumenthal, D. J; Juodawlkis, P. W; Loh, W.; Sorace-Agaskar, C.; Jones, A. E; Balram, K. C; Matthews, J. C F; Laing, A.; et al. 2022 roadmap on integrated quantum photonics. *Journal of Physics: Photonics* **2022**, *4* (1), 012501.
- (2) Elshaari, A. W.; Pernice, W.; Srinivasan, K.; Benson, O.; Zwiller, V. Hybrid integrated quantum photonic circuits. *Nat. Photonics* **2020**, *14* (5), 285–298.
- (3) Reddy, D. V.; Lita, A. E.; Nam, S.; Mirin, R. P.; Verma, V. B. Achieving 98% system efficiency at 1550 nm in superconducting nanowire single photon detectors. In *Proc. Rochester Conf. Coherence Quantum Opt. CQO 2019*, Optical Society of America, 2019, page W2B.2.
- (4) Chiles, J.; Charaev, I.; Lasenby, R.; Baryakhtar, M.; Huang, J.; Roshko, A.; Burton, G.; Colangelo, M.; Van Tilburg, K.; Arvanitaki, A.; Nam, S. W.; Berggren, K. K. New constraints on dark photon dark matter with superconducting nanowire detectors in an optical haloscope. *Phys. Rev. Lett.* **2022**, *128* (23), 231802.
- (5) Korzh, B.; Zhao, Q.-Y.; Allmaras, J. P.; Frasca, S.; Autry, T. M.; Bersin, E. A.; Beyer, A. D.; Briggs, R. M.; Bumble, B.; Colangelo, M.; et al. Demonstration of sub-3 ps temporal resolution with a superconducting nanowire single-photon detector. *Nat. Photonics* **2020**, *14* (4), 250–255.

- (6) Ferrari, S.; Schuck, C.; Pernice, W. Waveguide-integrated superconducting nanowire single-photon detectors. *Nanophotonics* **2018**, *7* (11), 1725–1758.
- (7) Pernice, W.H.P.; Schuck, C.; Minaeva, O.; Li, M.; Goltsman, G.N.; Sergienko, A.V.; Tang, H.X. High-speed and high-efficiency travelling wave single-photon detectors embedded in nanophotonic circuits. *Nat. Commun.* **2012**, *3* (1), 1325.
- (8) Vetter, A.; Ferrari, S.; Rath, P.; Alaee, R.; Kahl, O.; Kovalyuk, V.; Diewald, S.; Goltsman, G. N.; Korneev, A.; Rockstuhl, C.; Pernice, W. H. P. Cavity-enhanced and ultrafast superconducting single-photon detectors. *Nano Lett.* **2016**, *16* (11), 7085–7092.
- (9) Kahl, O.; Ferrari, S.; Kovalyuk, V.; Goltsman, G. N.; Korneev, A.; Pernice, W. H. P. Waveguide integrated superconducting single-photon detectors with high internal quantum efficiency at telecom wavelengths. *Sci. Rep.* **2015**, *5* (1), 1–11.
- (10) Beyer, A. D.; Briggs, R. M.; Marsili, F.; Cohen, J. D.; Meenehan, S. M.; Painter, O. J.; Shaw, M. D. Waveguide-coupled superconducting nanowire single-photon detectors. 2015 Conference on Lasers and Electro-Optics (CLEO), IEEE, 2015, pages 1–2.
- (11) Najafi, F.; Mower, J.; Harris, N. C.; Bellei, F.; Dane, A.; Lee, C.; Hu, X.; Kharel, P.; Marsili, F.; Assefa, S.; Berggren, K. K.; Englund, D. On-chip detection of non-classical light by scalable integration of single-photon detectors. *Nat. Commun.* **2015**, *6* (1), 1–8.
- (12) Kahl, O.; Ferrari, S.; Rath, P.; Vetter, A.; Nebel, C.; Pernice, W. H. P. High efficiency on-chip single-photon detection for diamond nanophotonic circuits. *Journal of Lightwave Technology* **2016**, 34 (2), 249–255.
- (13) Sprengers, J. P.; Gaggero, A.; Sahin, D.; Jahanmirinejad, S.; Frucci, G.; Mattioli, F.; Leoni, R.; Beetz, J.; Lermer, M.; Kamp, M.; Hofling, S.; Sanjines, R.; Fiore, A. Waveguide superconducting single-photon detectors for integrated quantum photonic circuits. *Appl. Phys. Lett.* **2011**, *99* (18), 181110.
- (14) Wolff, M. A.; Vogel, S.; Splitthoff, L.; Schuck, C. Superconducting nanowire single-photon detectors integrated with tantalum pentoxide waveguides. *Sci. Rep.* **2020**, *10* (1), 1–9.
- (15) Zhang, M.; Wang, C.; Cheng, R.; Shams-Ansari, A.; Loncar, M. Monolithic ultra-high-q lithium niobate microring resonator. *Optica* **2017**, *4* (12), 1536–1537.
- (16) Holzgrafe, J.; Sinclair, N.; Zhu, D.; Shams-Ansari, A.; Colangelo, M.; Hu, Y.; Zhang, M.; Berggren, K. K.; Loncar, M. Cavity electro-optics in thin-film lithium niobate for efficient microwave-to-optical transduction. *Optica* **2020**, *7* (12), 1714–1720.
- (17) Wang, C.; Zhang, M.; Chen, X.; Bertrand, M.; Shams-Ansari, A.; Chandrasekhar, S.; Winzer, P.; Loncar, M. Integrated lithium niobate electro-optic modulators operating at cmos-compatible voltages. *Nature* **2018**, *562* (7725), 101–104.
- (18) Shao, L.; Yu, M.; Maity, S.; Sinclair, N.; Zheng, L.; Chia, C.; Shams-Ansari, A.; Wang, C.; Zhang, M.; Lai, K.; Loncar, M. Microwave-to-optical conversion using lithium niobate thin-film acoustic resonators. *Optica* **2019**, *6* (12), 1498–1505.
- (19) Zhu, D.; Shao, L.; Yu, M.; Cheng, R.; Desiatov, B.; Xin, C. J.; Hu, Y.; Holzgrafe, J.; Ghosh, S.; Shams-Ansari, A.; Puma, E.; Sinclair, N.; Reimer, C.; Zhang, M.; Loncar, M. Integrated photonics on thinfilm lithium niobate. *Advances in Optics and Photonics* **2021**, *13* (2), 242–352.
- (20) Sayem, A. A.; Cheng, R.; Wang, S.; Tang, H. X. Lithium-niobate-on-insulator waveguide-integrated superconducting nanowire single-photon detectors. *Appl. Phys. Lett.* **2020**, *116* (15), 151102.
- (21) Colangelo, M.; Desiatov, B.; Zhu, D.; Holzgrafe, J.; Medeiros, O.; Loncar, M.; Berggren, K. K. Superconducting nanowire single-photon detector on thin-film lithium niobate photonic waveguide. *CLEO: Science and Innovations*, Optical Society of America, 2020, p SM40–4.
- (22) Lomonte, E.; Wolff, M. A.; Beutel, F.; Ferrari, S.; Schuck, C.; Pernice, W. H. P.; Lenzini, F. Single-photon detection and cryogenic reconfigurability in lithium niobate nanophotonic circuits. *Nat. Commun.* **2021**, *12* (1), 1–10.
- (23) Gerritsen, S. H.; Chittock, N. J.; Vandalon, V.; Verheijen, M. A.; Knoops, H. C. M.; Kessels, W. M. M.; Mackus, A. J. M. Surface

- smoothing by atomic layer deposition and etching for the fabrication of nanodevices. ACS Applied Nano Materials 2022, 5 (12), 18116–18126
- (24) Häyrinen, M.; Bera, A.; Roussey, M.; Kuittinen, M.; Honkanen, S. Ald-tuned titanium dioxide nanophotonics. *Nanotechnology VII*; SPIE, **2015**; Vol. 9519, p 951903.
- (25) Alasaarela, T.; Korn, D.; Alloatti, L.; Saynatjoki, A.; Tervonen, A.; Palmer, R.; Leuthold, J.; Freude, W.; Honkanen, S. Reduced propagation loss in silicon strip and slot waveguides coated by atomic layer deposition. *Opt. Express* **2011**, *19* (12), 11529–11538.
- (26) Charaev, I.; Morimoto, Y.; Dane, A.; Agarwal, A.; Colangelo, M.; Berggren, K. K. Large-area microwire mosi single-photon detectors at 1550 nm wavelength. *Appl. Phys. Lett.* **2020**, *116* (24), 242603.
- (27) Zhang, X.; Charaev, I.; Liu, H.; Zhou, T. X; Zhu, D.; Berggren, K. K; Schilling, A. Physical properties of amorphous molybdenum silicide films for single-photon detectors. *Supercond. Sci. Technol.* **2021**, *34* (9), 095003.
- (28) Colangelo, M.; Korzh, B.; Allmaras, J. P.; Beyer, A. D.; Mueller, A. S.; Briggs, R. M.; Bumble, B.; Runyan, M.; Stevens, M. J.; McCaughan, A. N.; et al. Impedance-matched differential superconducting nanowire detectors. *Physical Review Applied* **2023**, *19* (4), 044093.
- (29) Luke, K.; Kharel, P.; Reimer, C.; He, L.; Loncar, M.; Zhang, M. Wafer-scale low-loss lithium niobate photonic integrated circuits. *Opt. Express* **2020**, 28 (17), 24452–24458.
- (30) Xiaolong Hu; Holzwarth, C.W.; Masciarelli, D.; Dauler, E.A.; Berggren, K.K. Efficiently coupling light to superconducting nanowire single-photon detectors. *IEEE Transactions on Applied Superconductivity* **2009**, *19* (3), 336–340.
- (31) Kovalyuk, V.; Hartmann, W.; Kahl, O.; Kaurova, N.; Korneev, A.; Goltsman, G.; Pernice, W. H. P. Absorption engineering of nbn nanowires deposited on silicon nitride nanophotonic circuits. *Opt. Express* **2013**, *21* (19), 22683–22692.
- (32) Ravindran, P.; Cheng, R.; Tang, H.; Bardin, J. C. Active quenching of superconducting nanowire single photon detectors. *Opt. Express* **2020**, 28 (3), 4099–4114.
- (33) Liu, N.; Mesch, M.; Weiss, T.; Hentschel, M.; Giessen, H. Infrared perfect absorber and its application as plasmonic sensor. *Nano Lett.* **2010**, *10* (7), 2342–2348.
- (34) Akhlaghi, M. K.; Schelew, E.; Young, J. F. Waveguide integrated superconducting single-photon detectors implemented as near-perfect absorbers of coherent radiation. *Nat. Commun.* **2015**, *6* (1), 8233.
- (35) Munzberg, J.; Vetter, A.; Beutel, F.; Hartmann, W.; Ferrari, S.; Pernice, W. H. P.; Rockstuhl, C. Superconducting nanowire single-photon detector implemented in a 2d photonic crystal cavity. *Optica* **2018**, *5* (5), 658–665.
- (36) Buzzi, A.; Castellani, M.; Foster, R. A.; Medeiros, O.; Colangelo, M.; Berggren, K. K. A nano cryotron memory and logic family. *Appl. Phys. Lett.* **2023**, *122* (14), na.
- (37) Foster, R. A.; Castellani, M.; Buzzi, A.; Medeiros, O.; Colangelo, M.; Berggren, K. K. A superconducting nanowire binary shift register. *Appl. Phys. Lett.* **2023**, *122* (15), na.
- (38) Castellani, M.; Owen, M.; Foster, R. A.; Buzzi, A.; Colangelo, M.; C Bienfang, J.; Restelli, A.; Berggren, K. K. A nanocryotron ripple counter integrated with a superconducting nanowire single-photon detector for megapixel arrays. *arXiv preprint arXiv:2304.11700* **2023**, na.
- (39) Colangelo, M.; Zhu, D.; Santavicca, D. F.; Butters, B. A.; Bienfang, J. C.; Berggren, K. K. Compact and tunable forward coupler based on high-impedance superconducting nanowires. *Physical Review Applied* **2021**, *15* (2), 024064.
- (40) Pelucchi, E.; Fagas, G.; Aharonovich, I.; Englund, D.; Figueroa, E.; Gong, Q.; Hannes, H.; Liu, J.; Lu, C.-Y.; Matsuda, N.; Pan, J.-W.; Schreck, F.; Sciarrino, F.; Silberhorn, C.; Wang, J.; Jons, K. D. The potential and global outlook of integrated photonics for quantum technologies. *Nature Reviews Physics* **2022**, *4* (3), 194–208.